

Intelligent Chameleonlike Metashells for Mass Diffusion

Zeren Zhang, Fubao Yang, and Jiping Huang[✉]

Department of Physics, State Key Laboratory of Surface Physics, and Key Laboratory of Micro and Nano Photonic Structures (MOE), Fudan University, Shanghai 200438, China



(Received 12 October 2022; revised 21 November 2022; accepted 23 December 2022; published 3 February 2023)

Metamaterials facilitate on-demand manipulations of mass diffusion and have been broadly employed in many fields covering optics, electronics, and particle dynamics. However, the applications of existing mass-diffusion metamaterials are severely limited due to the lack of intelligence when it comes to dynamic environments. To solve the problem, we bestow intelligence on metashells by utilizing transformation-invariant metamaterials, thus proposing intelligent chameleonlike metashells for mass diffusion. Such metashells not only automatically change their efficient parameters to adapt to environmental change but also cost no energy. Based on it, we further design an irregular-shaped chameleonlike concentrator and circular chameleonlike rotator. Meanwhile, we offer experimental suggestions combined with layered structure devices to validate our proposal as well. Our study may be an inspiration for intelligentizing mass-diffusion metamaterials in electronics and plasma physics.

DOI: 10.1103/PhysRevApplied.19.024009

I. INTRODUCTION

Metamaterials for mass diffusion have aroused wide attention since the particle cloak based on transformation theory was proposed [1–3], because the potential applications in an actual scenario like drug delivery are very promising. To date, numerous fundamental devices to manipulate mass diffusion ranging from particle transport to light propagation have been reported, such as particle concentrator [4–7], electron cloak [8], light-diffusive cloak [9–11], plasma rotator [12], etc. Moreover, exceptional points and geometry phases were found in a diffusion-convection system recently [13], suggesting a possibility for studying topological physics in mass diffusion [14–18].

Although conventional mass-diffusive metamaterials have achieved great success, they still face the severe challenge of lacking intelligence. In other words, the designed metamaterials fail to adaptively respond to environment change because their key parameters are usually fixed according to the transformation theory [19,20]. This fact causes a fatal limitation where one device works only for a specific environment. Studying self-adapting metamaterials for mass diffusion is of great value accordingly. Transformation-invariant metamaterial is a potential choice.

Transformation-invariant metamaterials, inspired by ϵ -near-zero media [21], refer to metamaterials with extreme anisotropy. Namely, the diffusivity of transformation-invariant metamaterials is nearly infinite

for one direction but nearly zero for the other. This unique property makes transformation-invariant metamaterials robust under arbitrary coordinates' transformation. Therefore, transformation-invariant metamaterials have been broadly studied in electromagnetism [22], acoustics [23,24], and thermotics [25–27]. Recently, it has been reported that metamaterials with high anisotropy are adaptable to the environment change, behaving like chameleons [28,29]. Utilizing transformation-invariant metamaterials, it is feasible to design chameleonlike metashells, which can effectively change their key parameters according to the environment change, being good candidates for intelligent devices.

In this work, we explain the robustness of transformation-invariant metamaterials under coordinates' transformation. We prove that the transformation-invariant metashells have adaptive responses when the background environment changes, thus called chameleonlike metashells. Then we further design an irregular-shaped concentrator and a circular rotator that intelligently adapt to environmental changes. We also provide experimental suggestions that layered structure is an excellent candidate for high anisotropy. Let us discuss the basic principle first.

II. THEORY OF CHAMELEONLIKE METASHIELDS

For brevity, we assume the chemical species solubilities are identical and ignore the effect of chemical potentials [30]. Thus, a passive and stable mass-diffusion process is dominated by Fick's law [31],

*jphuang@fudan.edu.cn

$$\nabla \cdot \left(-\overset{\leftrightarrow}{D} \nabla c \right) = 0, \quad (1)$$

where c is the volume concentration and $\overset{\leftrightarrow}{D}$ is the diffusivity. We can explain the transparency of transformation-invariant metamaterials with transformation theory, whose physical pictures are illustrated in Fig. 1. When we stretch a circle line [denoted by a green line in Fig. 1(a)] to an annulus in the virtual space, the diffusivity of the annulus becomes extremely anisotropic, i.e., $D_{rr} \approx \infty$, $D_{\theta\theta} \approx 0$. Meanwhile, the existence of the annulus does not affect the outside environment, exhibiting transparency behavior. Next, we prove in detail that the transparency of the transformation-invariant metamaterials does not change under any finite coordinate transformation. Let us consider arbitrary two-dimensional (2D) coordinate transformation

in cylindrical coordinates [32,33],

$$\begin{aligned} r' &= f(r, \theta) \\ \theta' &= g(r, \theta), \end{aligned} \quad (2)$$

where $f(r, \theta)$ and $g(r, \theta)$ are separately arbitrary functions of radius r and angle θ . Then the Jacobian matrix \mathbf{J} is written as,

$$\mathbf{J} = \begin{bmatrix} \partial_r f & \partial_\theta f / r \\ r' \partial_r g & r' \partial_\theta g / r \end{bmatrix}. \quad (3)$$

Then the transformed diffusivity $\overset{\leftrightarrow}{D}'$ can be obtained according to the transformation theory $\overset{\leftrightarrow}{D}' = \mathbf{J} \overset{\leftrightarrow}{D} \mathbf{J}^\tau / \det \mathbf{J}$

$$= \frac{1}{\det \mathbf{J}} \begin{bmatrix} D_{rr}(\partial_r f)^2 + D_{\theta\theta}(\partial_\theta f / r)^2 \\ D_{rr}\partial_r f (r' \partial_r g) + D_{\theta\theta}(\partial_\theta f / r)(r' \partial_\theta g / r) \end{bmatrix}, \quad (4)$$

where $\det \mathbf{J}$ is the determinant of \mathbf{J} , \mathbf{J}^τ is the transpose of \mathbf{J} . D_{rr} and $D_{\theta\theta}$ are the radial and tangential components of diffusivity, respectively. Then the eigenvalues of $\overset{\leftrightarrow}{D}'$ can be calculated as

$$\lambda_1 = \frac{D_{rr}}{\det \mathbf{J}} [(\partial_r f)^2 + (r' \partial_r g)^2], \quad (5a)$$

$$\lambda_2 \approx \frac{D_{\theta\theta}}{\det \mathbf{J}}. \quad (5b)$$

Note that $D_{rr} \approx \infty$ and $D_{\theta\theta} \approx 0$ for transformation-invariant metamaterials. Equation (5) can be further reduced to

$$\lambda_1 \approx \infty, \quad (6a)$$

$$\lambda_2 \approx 0. \quad (6b)$$

Equation (6) indicates the eigenvalues can keep unchanged under arbitrary coordinate transformations. Namely, the transformation-invariant metamaterials are robust under coordinates' transformation.

Now we are in a position to prove the chameleonlike property of transformation-invariant metamaterials. Here, we treat the whole system as three regions with diffusivities of $\overset{\leftrightarrow}{D}_1$, $\overset{\leftrightarrow}{D}_2$, and $\overset{\leftrightarrow}{D}_3$, as shown in Fig. 1(b1). The mass concentration of region 1, region 2, and region 3 is denoted as c_1 , c_2 , and c_3 , respectively. We then resolve Eq. (1) directly under cylindrical coordinates. Thus, Eq. (1) can

be expressed as

$$\frac{1}{r} \partial_r (r D_{rr} \partial_r c) + \frac{1}{r} \partial_\theta \left(\frac{D_{\theta\theta}}{r} \partial_\theta c \right) = 0. \quad (7)$$

For brevity, we set diffusivity $\overset{\leftrightarrow}{D}_1 = \overset{\leftrightarrow}{D}_3 = \text{constant}$. And $\overset{\leftrightarrow}{D}_2 = \text{diag}[D_{rr}, D_{\theta\theta}]$. Then, the general solution of Eq. (7) is

$$c = A_0 + B_0 \ln r + \sum_{p=1}^{\infty} [A_p \cos(p\theta) + B_p \sin(p\theta)] r^{p\eta} \quad (8)$$

$$+ \sum_{q=1}^{\infty} [C_q \cos(q\theta) + D_q \sin(q\theta)] r^{-q\eta}, \quad (8)$$

where $\eta = \sqrt{D_{\theta\theta}/D_{rr}}$. And the boundary conditions can be easily derived as

$$\begin{aligned} c_1|_{r \rightarrow 0} &\text{ is finite,} \\ c_1|_{r=r_1} &= c_2|_{r=r_1}, \\ c_2|_{r=r_2} &= c_3|_{r=r_2}, \\ -D_1 \partial_r c_1|_{r=r_1} &= -D_{rr} \partial_r c_2|_{r=r_1}, \\ -D_{rr} \partial_r c_2|_{r=r_2} &= -D_3 \partial_r c_3|_{r=r_2}, \\ c_3|_{r \rightarrow \infty} &= -\nabla c r \cos \theta. \end{aligned} \quad (9)$$

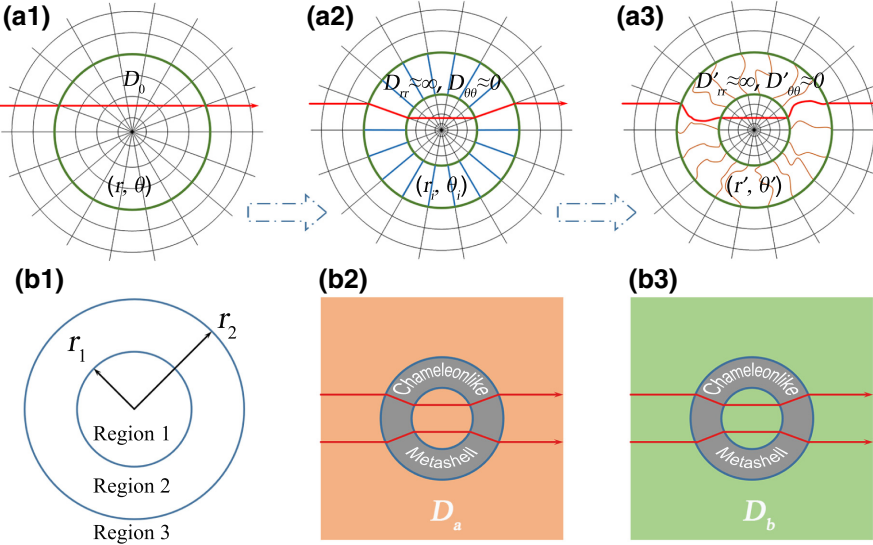


FIG. 1. (a1)–(a3) Understanding transformation invariance with transformation theory. (a1) Normal material before transforming. (a2) Transformed material with extremely anisotropic diffusivity. (a3) Transformed material with an invariant eigenvalue under a further coordinate transformation. The red line represents the mass flow. (b1)–(b3) Schematic diagrams of chameleonlike behavior. (b1) A core-shell structure. (b2),(b3) Chameleonlike concentrator working in environments with diffusivity D_a and D_b , respectively. Here $D_a \neq D_b$. The red line denotes the mass flow.

Then we can obtain the effective diffusivity of core-shell structure (region 1 and 2) as [34,35]

$$D_e = \eta D_{rr} \frac{(1 + \xi^\eta) D_3 + (1 - \xi^\eta) \eta D_{rr}}{(1 - \xi^\eta) D_3 + (1 + \xi^\eta) \eta D_{rr}}, \quad (10)$$

where $\xi = r_1^2/r_2^2$. We can find the effective diffusivity $D_e \approx D_3$ after substituting the diffusivity of the transformation-invariant metamaterials. It means that the effective diffusivity of the core-shell structure can accordingly change with the environment, which is the so-called chameleonlike behavior. As shown in Figs. 1(b2) and 1(b3), the transformation-invariant metashell adjusts itself to adapt to different backgrounds. It should be highlighted that the chameleonlike behavior expends no external energy according to the deducing process.

As shown in Figs. 1(a1) and 1(a2), transformation-invariant metashells have compressed the space so that they possess a converging effect naturally. Hence, we design an irregular-shaped chameleonlike rotator and a circular chameleonlike rotator with transformation-invariant metamaterials to validate the advantages over conventional devices. For the irregular-shaped chameleonlike concentrator, an annulus region is twisted into an irregular-shaped one in the virtual space. The coordinate transformation can be expressed as

$$\begin{aligned} r' &= rF(\theta), \quad r_1 < r < r_2 \\ \theta' &= \theta, \end{aligned} \quad (11)$$

in which $F(\theta) = 1.2 + 0.5 \sin(\theta) + 0.5 \cos(2\theta)$. r_1 and r_2 are the inner and outer radii of the annulus, respectively. Then the transformed diffusivity of the metashell can be obtained by referring to Eqs. (4) and (11). The schematic diagram for the transformation-invariant concentrator can be found in Fig. 7(a) in the Appendix.

The coordinates' transformation for the normal concentrator with the same shape is [19]

$$\begin{aligned} r' &= \frac{r_1}{r_m} r, \quad r' < r_1 F(\theta), \\ r' &= Ar + BF(\theta), \quad r_1 F(\theta) < r' < r_2 F(\theta), \\ \theta' &= \theta, \end{aligned} \quad (12)$$

where r_m is a constant. $F(\theta) = 1.2 + 0.5 \sin(\theta) + 0.5 \cos(2\theta)$, $A = (r_2 - r_1)/(r_2 - r_m)$, and $B = (r_1 - r_m)r_2/(r_2 - r_m)$. Hence, the transformed diffusivity of the metashell is [27]

$$\overset{\leftrightarrow}{D}' = D_b \begin{bmatrix} D_{11} & D_{12} \\ D_{21} & D_{22} \end{bmatrix}, \quad (13)$$

where the components D_{ij} are

$$\begin{aligned} D_{11} &= \frac{(r_2 - r_m)r' + r_2(r_m - r_1)F(\theta)}{(r_2 - r_m)r'} \\ &+ \frac{r_2^2(r_m - r_1)^2 (dF(\theta)/d\theta)^2}{[(r_2 - r_m)^2 r' + r_2(r_m - r_1)(r_2 - r_m)F(\theta)] r'}, \end{aligned}$$

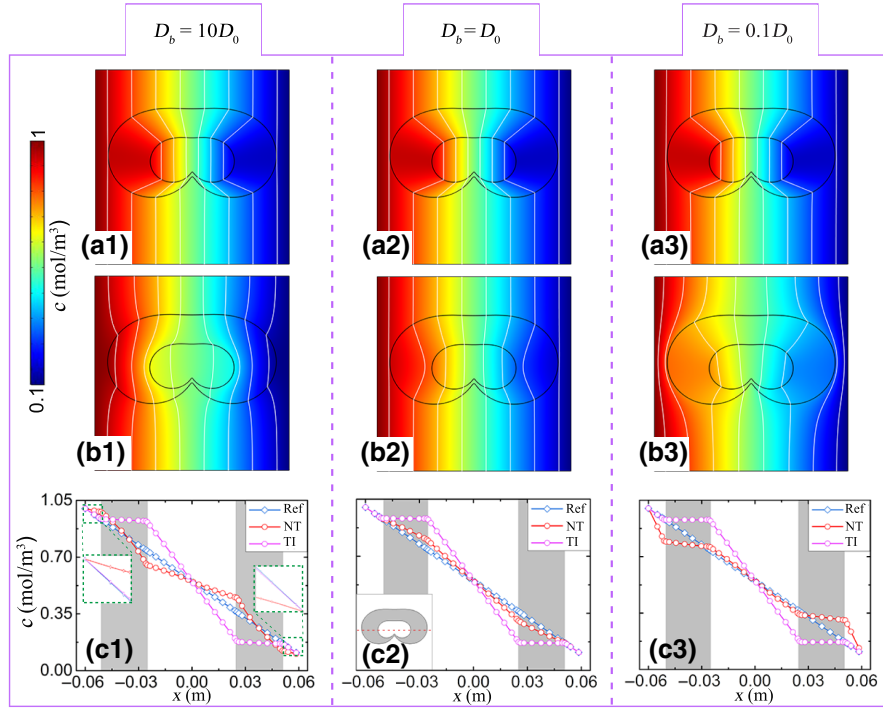


FIG. 2. (a1)–(a3) Simulations of the transformation-invariant concentrator. Background diffusivity (a1) $10D_0$, (a2) D_0 , and (a3) $0.1D_0$. (b1)–(b3) Simulations of the normal-transforming concentrator. Background diffusivity (b1) $10D_0$, (b2) D_0 , and (b3) $0.1D_0$. White lines are isoconcentrates. The flow direction is along x axis. (c1)–(c3) Comparison between reference, transformation-invariant concentrator, and normal-transforming concentrator. TI denotes transformation-invariant concentrator and NT denotes normal-transforming concentrator. Background diffusivity (c1) $10D_0$, (c2) D_0 , and (c3) $0.1D_0$. We set two boundary conditions as $c_h = 1 \text{ mol m}^{-3}$ and $c_l = 0.1 \text{ mol m}^{-3}$. The green dashed squares in (c1) are enlarged images. The inset in (c2) denotes the data extraction position. The side length of the background is $l = 0.12 \text{ m}$. Other parameters: $r_1 = 0.015 \text{ m}$, $r_m = 0.0029 \text{ m}$, $r_2 = 0.003 \text{ m}$, $D_{rr} = 1 \times 10^{-5} \text{ m s}^{-1}$, $D_{\theta\theta} = 1 \times 10^{-12} \text{ m s}^{-1}$.

$$D_{12} = D_{21} = \frac{r_2(r_1 - r_m)(dF(\theta)/d\theta)}{(r_2 - r_m)r' + r_2(r_m - r_1)F(\theta)},$$

$$D_{22} = \frac{(r_2 - r_m)r'}{(r_2 - r_m)r' + r_2(r_m - r_1)F(\theta)}. \quad (14)$$

It should be noted that a larger ratio (r_m/r_1) would bring a higher converging effect, and the maximum boundary of the ratio is r_2/r_1 . For the transformation-invariant concentrator, the ratio r_m/r_1 approximately equals r_2/r_1 , which accounts for its bigger concentration gradient in the core region.

For the chameleonlike rotator, the coordinate transformation is

$$r' = r,$$

$$\theta' = \theta + \theta_0(r - r_2)/(r_1 - r_2), \quad r_1 < r < r_2, \quad (15)$$

where θ_0 is the rotating angle. This coordinate's transformation can be explained by rotating a series of circles at different angles whose values are determined by the corresponding radii. Similarly, we can derive the transformed diffusivity according to Eqs. (4) and (15). It should

be noted that the designed rotator possesses both functions of converging and rotating mass flow, which has been reflected from Figs. 1(a1) and 1(a2). The coordinates' transformation for a normal rotator can be found in the Appendix.

III. SIMULATIONS

We carry out simulations with COMSOL Multiphysics to verify the theory. The model parameters are set as follows. A higher constant concentration source is applied to the left boundary of the box. A lower one is set as the opposite (right) side. We also set isolated conditions on the upper and lower boundaries. Further, we set the background diffusivity as D_b . Then we set diffusivities for transformation-invariant and normal-transforming metashell as $\text{diag}(10^{-5}, 10^{-12})$ and $5 \times 10^{-8} \text{ m s}^{-1}$, respectively. The corresponding transformed diffusivity can be calculated according to Eqs. (4) and (14). First, let us focus on the results of the chameleonlike concentrator. See Figs. 2 and 3. The performances of transformation-invariant metashell and normal-transforming metashell in the background with different diffusivity are exhibited.

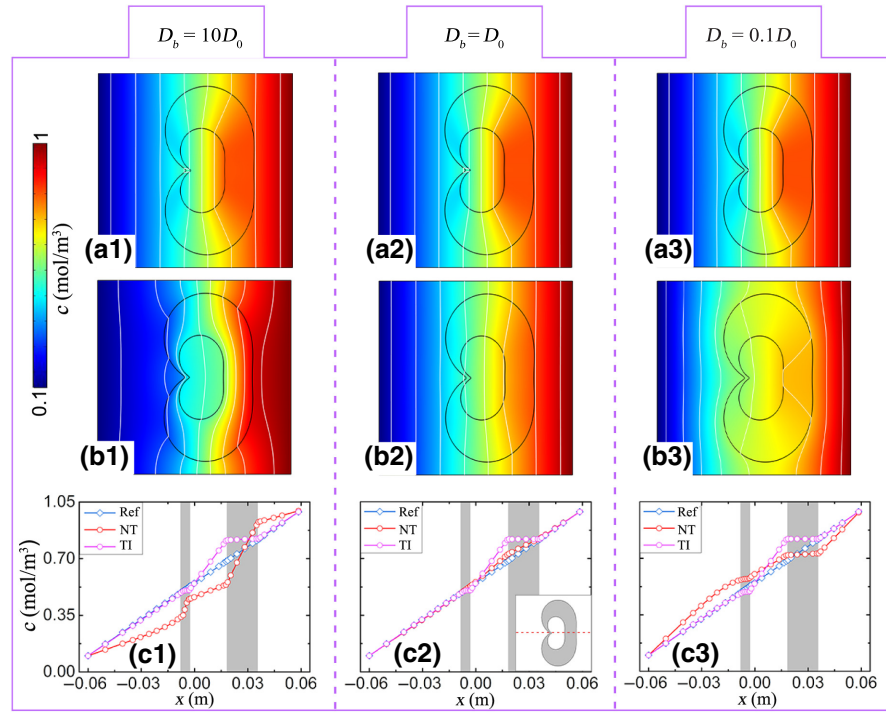


FIG. 3. (a1)–(a3) Simulations of the transformation-invariant concentrator. Background diffusivity (a1) $10D_0$, (a2) D_0 , and (a3) $0.1D_0$. (b1)–(b3) Simulations of the normal-transforming concentrator. Background diffusivity (b1) $10D_0$, (b2) D_0 , and (b3) $0.1D_0$. White lines are isoconcentrates. The flow direction is along $-y$ axis. (c1)–(c3) Comparison between reference, transformation-invariant concentrator, and normal-transforming concentrator. TI denotes transformation-invariant concentrator and NT denotes normal-transforming concentrator. The inset in (c2) denotes the data-extraction position. Background diffusivity (c1) $10D_0$, (c2) D_0 , and (c3) $0.1D_0$.

The proposed chameleonlike concentrator is only symmetrical in x axis. Therefore, we employ two simulations where the mass flow direction is along x or $-y$ axis, to remove the influence of symmetry. Figure 2 shows the results of mass flow towards x axis. In Fig. 2, the first and second rows illustrate the transformation-invariant and normal-transforming concentrator results, respectively. The second column shows the concentration distribution for the background diffusivity $D_b = D_0 = 5 \times 10^{-8} \text{ m s}^{-1}$, while the first and third columns show the cases of $D_b = 10D_0$ and $D_b = 0.1D_0$, respectively. From Figs. 2(b1)–2(b3), the isoconcentrates are disturbed with D_b increased or decreased, which indicates the normal-transforming concentrator fails after changing the background diffusivity. In contrast, the transformation-invariant concentrator always keeps working no matter whether increasing or decreasing the background diffusivity, as shown in Figs. 2(a1)–2(a3).

We also plot point graphs to compare the performances of normal-transforming and transformation-invariant concentrators more clearly, which are illustrated in Figs. 2(c1)–2(c3). The data is extracted from the position (at $y = 0$) denoted by a red dashed line in the inset of Fig. 2(c2). The gray region represents the metashell. The purple dot line represents the concentration profile with

the transformation-invariant metashell, while the red dot line represents the profile with the normal-transforming metashell. The blue square line denotes a pure homogeneous background's concentration profile. The red line overlaps the blue line outside the shell only in Fig. 2(c2), indicating normal-transforming concentrator only works for $D_b = D_0$. However, the well overlapping between the purple and blue line outside the shell reflects that the transformation-invariant concentrator does not disturb the background despite changing background diffusivity, which consists with the theory. Moreover, the larger concentration gradient of the purple dot line than that of the reference indicates that the transformation-invariant concentrator can indeed converge mass flow. Note that the purple dot line is steeper than the red one in the core region. The converging effect is determined by the ratio r_m/r_1 , as shown in the Appendix. The transformation-invariant concentrator has an equivalently larger ratio compared to the normal-transforming concentrator. Hence, the concentration gradient of the transformation-invariant concentrator is bigger.

Simulations for mass flow towards $-y$ axis are presented in Fig. 3. Similar to Figs. 2, 3(a1)–3(a3) are the simulations of transformation-invariant concentrator with $D_b = 10D_0$, $D_b = D_0$, and $D_b = 0.1D_0$,

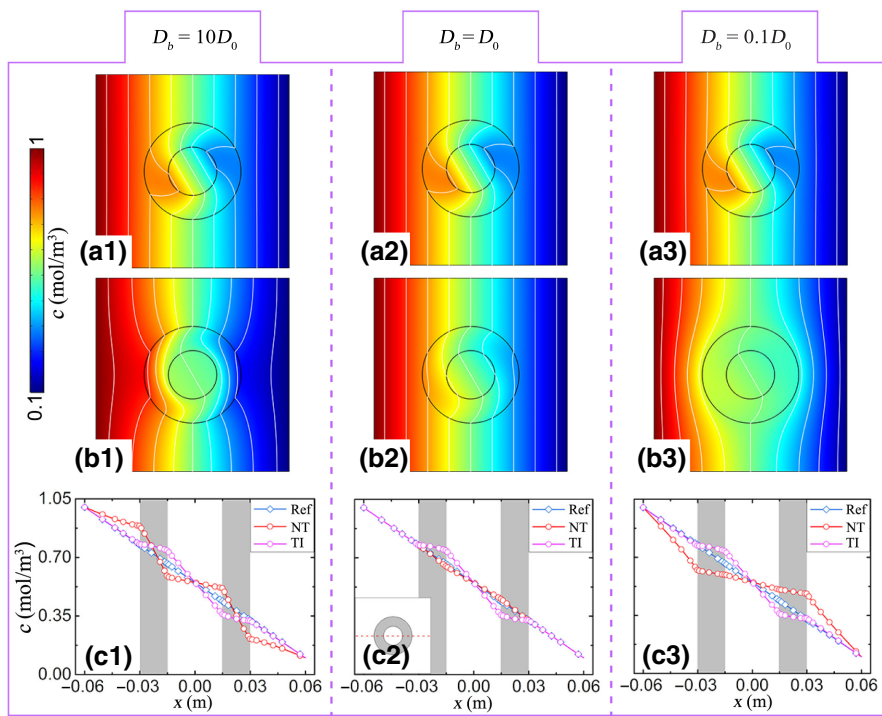


FIG. 4. (a1)–(a3) Simulations of the transformation-invariant rotator. Background diffusivity (a1) $10D_0$, (a2) D_0 , and (a3) $0.1D_0$. (b1)–(b3) Simulations of the normal-transforming rotator. Background diffusivity (b1) $10D_0$, (b2) D_0 , and (b3) $0.1D_0$. White lines are isoconcentrates. (c1)–(c3) Comparison between reference, transformation-invariant rotator, and normal-transforming rotator. TI denotes transformation-invariant rotator, and NT denotes normal-transforming rotator. Background diffusivity (c1) $10D_0$, (c2) D_0 , and (c3) $0.1D_0$. The inset in (c2) denotes the data extraction position. Here, $\theta_0 = \pi/6$.

respectively. Figures 3(b1)–3(b3) are the simulations of normal-transforming concentrator with $D_b = 10D_0$, $D_b = D_0$, and $D_b = 0.1D_0$, respectively. Figures 3(c1)–3(c3) are the data comparison between reference, normal-transforming concentrator, and transformation-invariant concentrator. Obviously, a different input direction of mass flow has no impact on the transformation-invariant or normal-transforming concentrator. Changing background diffusivity disables the normal-transforming concentrator, while the transformation-invariant concentrator keeps a good performance. Therefore, the proposed irregular transformation-invariant concentrator does have chameleonlike properties as the theory predicted.

Next, the results of chameleonlike rotator are shown in Fig. 4. Figures 4(a1)–4(a3) reflect that transformation-invariant rotator can adaptively respond to environment changes compared to Figs. 4(b1)–4(b3). And the direction of mass flow in the core region is guided at will. The rotating angle is determined by θ_0 , in good agreement with Eq. (15). Figures 4(c1)–4(c3) show that the transformation-invariant rotator exactly keeps background concentration unchanged, which further demonstrates the validity of the chameleonlike rotator. In addition, the concentration gradient in the core of the transformation-invariant rotator is bigger than that of the normal-transforming rotator attributed to the property of transformation-invariant metashell, as mentioned afore.

IV. DISCUSSION AND CONCLUSIONS

Although the material with extreme anisotropy is uncommon in the nature, we can employ two isotropic

materials whose diffusivities vary greatly to achieve approximately the same effect [36]. As shown in Fig. 5(a), we come up with a chameleonlike concentrator and rotator referring to the multilayered structure. Diffusivities of two isotropic materials are separately 10^{-5} and 10^{-12} m s\$^{-1}\$. Figures 5(b1)–5(b3) are the simulations for multilayered concentrator in different background diffusivity. Figures 5(c1)–5(c3) are the simulations for the multilayered rotator. The proposed structure obviously presents a reasonable performance for responding to background changes, indicating good experimental feasibility. Moreover, the devices with denser layers shall be closer to the ideal models.

We also provide simplified experimental suggestions to prove the designation qualitatively. Take the concentrator as an example. In Fig. 6, the background medium with a chessboard structure and the metashell are both composed of two materials with high (D_h) and low (D_l) diffusivities. We guess water and resin may be good candidates. The experimental equipment can be designed with two parts [37]. One part offers concentration sources with two tanks at the left and right ends. Each tank is filled with solution and deionized water, respectively, to produce a concentration gradient. The remaining part is background media with chessboard structure. Effective diffusivities of the background media can be calculated according to the Maxwell-Garnett formula, according to Eq. (A2) in the Appendix. Figures 6(a1) and 6(b1) are the schematic diagrams of chessboard structure of devices. With different filling factors, the effective diffusivity will be different. Figures 6(a2) and 6(b2) exhibit simulations of multilayered concentrator in background media with different

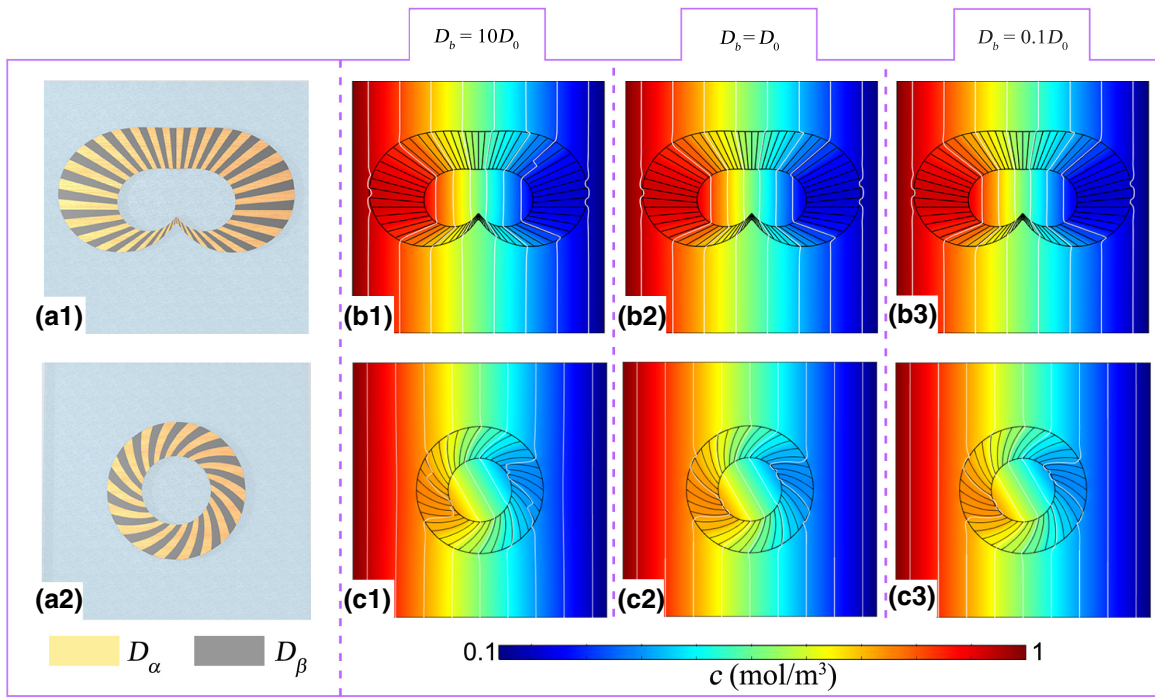


FIG. 5. Multilayered schematic diagrams of concentrator (a1) and rotator (a2). (b1)–(b3) Simulations of the multilayered transformation-invariant concentrator. Background diffusivity (b1) $10D_0$, (b2) D_0 , and (b3) $0.1D_0$. (b1)–(b3) Simulations of the multilayered transformation-invariant rotator. Background diffusivity (b1) $10D_0$, (b2) D_0 , and (b3) $0.1D_0$. White lines are isoconcentrates. And $D_\alpha = 1 \times 10^{-5} \text{ m s}^{-1}$, $D_\beta = 1 \times 10^{-12} \text{ m s}^{-1}$.

diffusivity. Note that the slight disturbance of the isoconcentrate in the background is caused by inadequately dense discretization of the chessboard. As a whole, the results accord well with the theory.

In conclusion, we transplant the transformation-invariant materials from optics (wave systems) to mass-diffusion systems. We also propose two kinds of metashells based on transformation-invariant metamaterials to

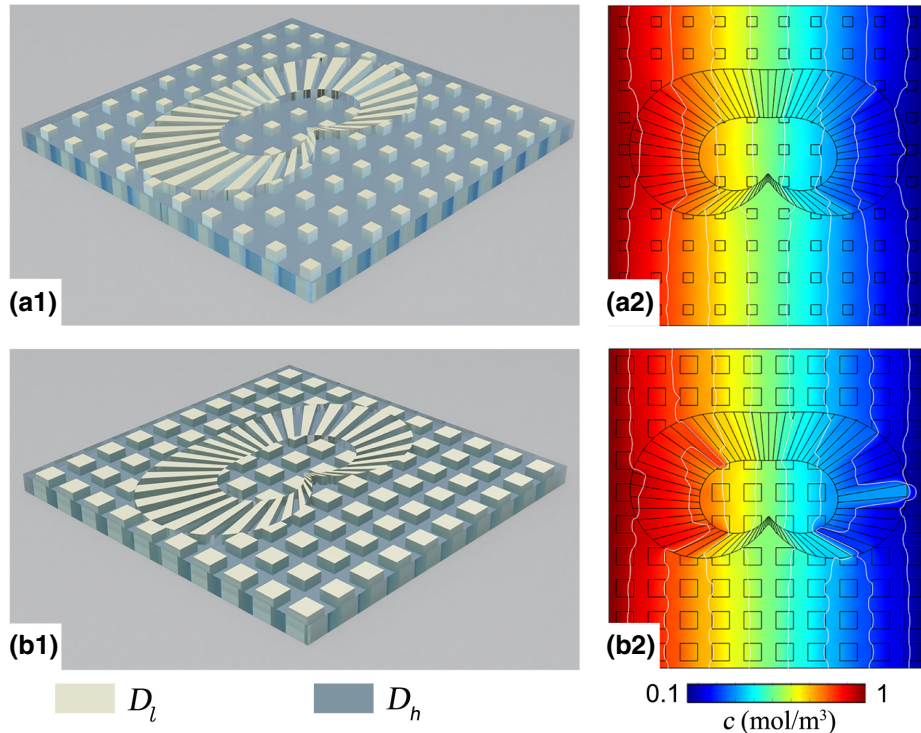


FIG. 6. (a1),(b1) Diagrammatic figures of the experimental setup with chessboard structure. (a2),(b2) Simulations of concentrator in backgrounds with chessboard structure (a1),(b1), respectively. White lines are isoconcentrates. And $D_l = 1 \times 10^{-12} \text{ m s}^{-1}$, $D_h = 1 \times 10^{-5} \text{ m s}^{-1}$. Filling factor f is 0.1 for (a1) and (a2); 0.3 for (b1) and (b2).

function as an intelligent chameleonlike concentrator and rotator, respectively. The devices are energy-free for responding to environmental change. Although we assume identical chemical species solubilities and ignore chemical potentials for brevity, the simulations are reliable. Excellent research has proved that the transformation theory is valid, considering solubilities and chemical potential [30]. Moreover, we provide suggestions to achieve chameleonlike devices experimentally. Our work may offer inspiration for studying intelligent metamaterials in mass-diffusion systems. And the physical picture can also be extended to more complicated systems, like the diffusion-convection system, which indicates a promising future.

ACKNOWLEDGMENTS

We acknowledge financial support from the National Natural Science Foundation of China under Grants No. 11725521 and No. 12035004, and from the Science and Technology Commission of Shanghai Municipality under Grant No. 20JC1414700.

APPENDIX

For the normal rotator, the coordinates' transformation is the same as the transformation-invariant rotator. Thus, the transformed diffusivity of the normal rotator is

$$\overset{\leftrightarrow}{D}' = D_b \begin{bmatrix} 1 & \frac{r'\theta_0}{r_1-r_2} \\ \frac{r'\theta_0}{r_1-r_2} & 1 + \left(\frac{r'\theta_0}{r_1-r_2} \right)^2 \end{bmatrix}. \quad (\text{A1})$$

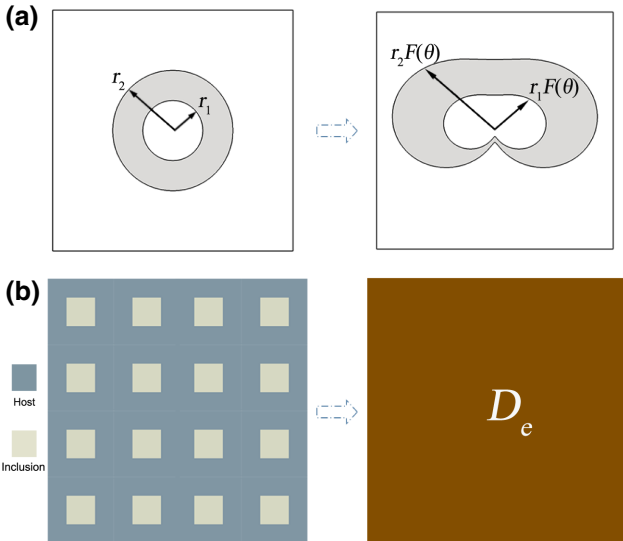


FIG. 7. (a) Coordinates transformation of the transformation-invariant concentrator. (b) Schematic diagram of Maxwell-Garnett formula.

Then the transformed parameters of the normal concentrator and rotator can be obtained by substituting \$D_b\$ into Eqs. (13) and (A1).

The effective medium theory gives an analytical model to approximately predict the macroscopic properties of composites, where the inclusions' volume fraction is determinant. As illustrated in Fig. 7(b), the inclusions are embedded in the host, and the whole system is equivalent to a homogeneous medium. The efficient diffusivity \$D_e\$ can be calculated according to the Maxwell-Garnett formula [35],

$$D_e = \frac{(1+f)D_i + (1-f)D_h}{(1-f)D_i + (1+f)D_h} D_h \quad (\text{A2})$$

in which \$f\$, \$D_i\$, and \$D_h\$ are the volume fraction of the inclusion, diffusivity of the inclusion, and diffusivity of the host, respectively. Then we can obtain different background diffusivities by changing the volume fraction \$f\$.

- [1] S. Guenneau and T. M. Puvirajasinghe, Fick's second law transformed: One path to cloaking in mass diffusion, *J. Royal Soc. Interface* **10**, 20130106 (2013).
- [2] L. Zeng and R. Song, Controlling chloride ions diffusion in concrete, *Sci. Rep.* **3**, 3359 (2013).
- [3] S. Guenneau, D. Petiteau, M. Zerrad, C. Amra, and T. Puvirajasinghe, Transformed Fourier and Fick equations for the control of heat and mass diffusion, *AIP Adv.* **5**, 053404 (2015).
- [4] J. M. Restrepo-Flórez and M. Maldovan, Mass separation by metamaterials, *Sci. Rep.* **6**, 21971 (2016).
- [5] X. Zhou, G. Xu, and H. Zhang, Binary masses manipulation with composite bilayer metamaterial, *Compos. Struct.* **267**, 113866 (2021).
- [6] Z. Zhang, L. Xu, and J. Huang, Controlling chemical waves by transforming transient mass transfer, *Adv. Theory Simul.* **5**, 2100375 (2021).
- [7] J. M. Restrepo-Flórez and M. Maldovan, Mass diffusion cloaking and focusing with metamaterials, *Appl. Phys. Lett.* **111**, 071903 (2017).
- [8] Y. Li, C. Liu, P. Li, T. Lu, C. Chen, Z. Guo, Y. Su, L. Qiao, J. Zhou, and Y. Bai, Scattering cancellation by a monolayer cloak in oxide dispersion-strengthened alloys, *Adv. Funct. Mater.* **30**, 2003270 (2020).
- [9] R. Schittny, M. Kadic, T. Bückman, and M. Wegener, Invisibility cloaking in a diffusive light scattering medium, *Science* **345**, 427 (2014).
- [10] R. Schittny, A. Niemeyer, F. Mayer, A. Naber, M. Kadic, and M. Wegener, Invisibility cloaking in light-scattering media, *Laser Photon. Rev.* **10**, 382 (2016).
- [11] B. Orazbayev, M. Beruete, A. Martínez, and C. García-Meca, Diffusive-light invisibility cloak for transient illumination, *Phys. Rev. A* **94**, 063850 (2016).
- [12] Z. Zhang and J. Huang, Transformation plasma physics, *Chin. Phys. Lett.* **39**, 075201 (2022).

- [13] L. Xu, G. Dai, G. Wang, and J. Huang, Geometric phase and bilayer cloak in macroscopic particle-diffusion systems, *Phys. Rev. E* **102**, 032140 (2020).
- [14] L. Xu, J. Wang, G. Dai, S. Yang, F. Yang, G. Wang, and J. Huang, Geometric phase, effective conductivity enhancement, and invisibility cloak in thermal convection-conduction, *Int. J. Heat Mass Transf.* **165**, 120659 (2021).
- [15] G. Xu, Y. Li, W. Li, S. Fan, and C.-W. Qiu, Configurable Phase Transitions in a Topological Thermal Material, *Phys. Rev. Lett.* **127**, 105901 (2021).
- [16] Y. Li, Y.-G. Peng, L. Han, M.-A. Miri, W. Li, M. Xiao, X.-F. Zhu, J. Zhao, A. Alù, S. Fan, and C.-W. Qiu, Antiparity-time symmetry in diffusive systems, *Science* **364**, 170 (2019).
- [17] L. Xu, G. Xu, J. Li, Y. Li, J. Huang, and C.-W. Qiu, Thermal Willis Coupling in Spatiotemporal Diffusive Metamaterials, *Phys. Rev. Lett.* **129**, 155901 (2022).
- [18] L. Xu, G. Xu, J. Huang, and C.-W. Qiu, Diffusive Fizeau Drag in Spatiotemporal Thermal Metamaterials, *Phys. Rev. Lett.* **128**, 145901 (2022).
- [19] S. Yang, J. Wang, G. Dai, F. Yang, and J. Huang, Controlling macroscopic heat transfer with thermal metamaterials: Theory, experiment and application, *Phys. Rep.* **908**, 1 (2021).
- [20] C. Z. Fan, Y. Gao, and J. P. Huang, Shaped graded materials with an apparent negative thermal conductivity, *Appl. Phys. Lett.* **92**, 251907 (2008).
- [21] M. Silveirinha and N. Engheta, Tunneling of Electromagnetic Energy Through Subwavelength Channels and Bends using Epsilon-Near-Zero Materials, *Phys. Rev. Lett.* **97**, 157403 (2006).
- [22] Y. Zhang, Y. Luo, J. B. Pendry, and B. Zhang, Transformation-Invariant Metamaterials, *Phys. Rev. Lett.* **123**, 067701 (2019).
- [23] L. Wu, M. Oudich, W. Cao, H. Jiang, C. Zhang, J. Ke, J. Yang, Y. Deng, Q. Cheng, T. Cui, and Y. Jing, Routing Acoustic Waves via a Metamaterial with Extreme Anisotropy, *Phys. Rev. Appl.* **12**, 044011 (2019).
- [24] M. H. Fakheri, A. Abdolali, and H. B. Sedeh, Arbitrary Shaped Acoustic Concentrators Enabled by Null Media, *Phys. Rev. Appl.* **13**, 034004 (2020).
- [25] Y. Liu, F. Sun, and S. He, Fast adaptive thermal buffering by a passive open shell based on transformation thermodynamics, *Adv. Theory Simul.* **1**, 1800026 (2018).
- [26] F. Sun, Y. Liu, Y. Yang, Z. Chen, and S. He, Thermal surface transformation and its applications to heat flux manipulations, *Opt. Express* **27**, 33757 (2019).
- [27] H. Barati Sedeh, M. H. Fakheri, A. Abdolali, F. Sun, and Y. Ma, Feasible Thermodynamics Devices Enabled by Thermal-Null Medium, *Phys. Rev. Appl.* **14**, 064034 (2020).
- [28] L. Xu, S. Yang, and J. Huang, Passive Metashells with Adaptive Thermal Conductivities: Chameleonlike Behavior and its Origin, *Phys. Rev. Appl.* **11**, 054071 (2019).
- [29] F. Yang, B. Tian, L. Xu, and J. Huang, Experimental Demonstration of Thermal Chameleonlike Rotators with Transformation-Invariant Metamaterials, *Phys. Rev. Appl.* **14**, 054024 (2020).
- [30] F. Avanzini, G. Falasco, and M. Esposito, Chemical cloaking, *Phys. Rev. E* **101**, 060102 (2020).
- [31] A. Fick, On liquid diffusion, *J. Membr. Sci.* **100**, 33 (1995).
- [32] J. B. Pendry, D. Schurig, and D. R. Smith, Controlling electromagnetic fields, *Science* **312**, 1780 (2006).
- [33] U. Leonhardt, Optical conformal mapping, *Science* **312**, 1777 (2006).
- [34] L. Xu and J. Huang, Electrostatic chameleons: Theory of intelligent metashells with adaptive response to inside objects, *Eur. Phys. J. B* **92**, 53 (2019).
- [35] L. Xu and J. Huang, Metamaterials for Manipulating Thermal Radiation: Transparency, Cloak, and Expander, *Phys. Rev. Appl.* **12**, 044048 (2019).
- [36] S. Narayana and Y. Sato, Heat Flux Manipulation with Engineered Thermal Materials, *Phys. Rev. Lett.* **108**, 214303 (2012).
- [37] Y. Li, C. Yu, C. Liu, Z. Xu, Y. Su, L. Qiao, J. Zhou, and Y. Bai, Mass diffusion metamaterials with “plug and switch” modules for ion cloaking, concentrating, and selection: Design and experiments, *Adv. Sci.* **9**, 2201032 (2022).